

SPARC HSBs, and LSBs, the surface density of dark matter haloes, and MOND.

Antonino Del Popolo¹

^a*Dipartimento di Fisica e Astronomia, University Of Catania, Viale Andrea Doria 6, 95125 Catania*
^b*Institute of Astronomy, Russian Academy of Sciences, 119017, Pyatnitskaya str., 48, Moscow, Russia*

Abstract

In this paper, we use SPARC's HSBs, and LSBs galaxies to verify two issues. The first one is related to one claim of [1] D09, namely: is the DM surface density (DMsd) a constant universal quantity, equal to $\log(\Sigma/M_{\odot}\text{pc}^{-2}) = 2.15 \pm 0.2$, or does it depend on the baryon surface density of the system? The second one, is based on a MOND prediction that for HSBs the DMsd is constant, and equal to $\log(\Sigma/M_{\odot}\text{pc}^{-2}) = 2.14$, while for LSBs the surface density is not constant and takes values that are smaller than for HSBs and D09 prediction [2]. We find that HSBs shows a constant DMsd vs magnitude as in D09, and a constant DMsd vs Σ_{eff} as in MOND prediction, for HSBs with $\Sigma_{\text{eff}} > 200L_{\odot}/\text{pc}^2$, and $\Sigma_{\text{eff}} > 300L_{\odot}/\text{pc}^2$. However, the value of the DMsd is larger, $\Sigma \simeq 2.61$ (in the case of the DMsd-magnitude with $\Sigma_{\text{eff}} > 300L_{\odot}/\text{pc}^2$), and $\Sigma \simeq 2.54$ (in the case of the surface DMsd-surface brightness with $\Sigma_{\text{eff}} > 200L_{\odot}/\text{pc}^2$). This value slightly depends on the threshold to determine whether a galaxy is HSB. In the case of LSBs, for $\Sigma_{\text{eff}} < 100L_{\odot}/\text{pc}^2$, and $\Sigma_{\text{eff}} < 25L_{\odot}/\text{pc}^2$, the surface density vs magnitude, for lower magnitudes, is approximately equal to that predicted by D09, but several galaxies, for magnitude $M > -17$ have smaller values than those predicted by D09. The DMsd vs Σ_{eff} shows a similar behavior in qualitative, but not quantitative, agreement with MOND predictions. In summary, in the case of HSBs both D09 and MOND are in qualitative, but not quantitative, agreement with the data. In the case of LSBs D09 is mainly in disagreement with the data, and MOND only in qualitative

*Antonino Del Popolo
Email address: antonino.delpopolo@unict.it (Antonino Del Popolo)

agreement with them.

Keywords: Galaxies; Alternative theory of gravity; galaxies surface density

1. Introduction

In spite of the fact that the Λ CDM model, is a very good model in describing the observations on intermediate scales [3, 4, 5, 6, 7, 8, 9], and cosmology scales [6, 7, 8], it shows several drawbacks. To start with we recall the cosmological constant problem [10, 11], and the cosmic coincidence problem [12]. Apart the mentioned problems several others are present. At large scale there is the unsolved tensions between the the current value of the Hubble parameter, H_0 , having different values when measured with different methods, for example using the CMB, and supernovae and stars in the relatively recent universe [13]. Moreover, there is another tension between the data of Planck 2015 and the σ_8 growth rate of perturbations [14], and with CFHTLenS weak lensing [15] data. In the large-angle fluctuations in the CMB are present a power hemispherical asymmetry [16, 17, 18, 19, 20, 21], a quadrupole-octupole alignment [22, 23, 24, 25, 26], and a cold spot [27, 28, 29].

Other problems are present on smaller scales ($\simeq 1 - 10$ kpcs). Those often recalled are the "Cusp/Core" problem, namely the discrepancy between the cuspy profiles obtained in dark matter (DM) only N-body simulations ([30, 31, 32], and the observations of dwarf spirals, dwarf spheroidals (dSphs), and Low Surface Brightness (LSBs) galaxies showing cored profiles ([33, 34, 35, 36, 37, 38, 39, 40, 36, 37, 38, 39, 41]) . The "missing satellite problem" consists in the discrepancy between the number of satellites or subhaloes predicted by DM only N-body simulations ([42, 43]), and the number of subhaloes really observed. Moreover, the subhaloes obtained in simulations are too dense with respect to those observed around the Milky Way [44, 45]. The last is dubbed "too-big-to-fail" problem. Finally, we cite the issue of the location on planes of satellite galaxies of the Milky Way and M31 [46], difficult to explain. This is dubbed "satellites planes problem", but recently [47] showed a solution. The quoted problems have been attacked from different fronts. Some authors proposed to modify

the power spectrum (e.g. [48]), others proposed to modify either the particles constituting DM ([49, 50, 51, 52]), or the theory of gravity ([53, 54, 55, 56, 57]). Apart these drastic solutions, other astrophysical solutions have been proposed. They are based on the role of baryons in “heating” DM. A well known mechanism is that related to supernovae feedback ([58, 59, 60, 61, 62]), and another one is related to the transfer of energy and angular momentum from baryons to DM through dynamical friction ([63, 64, 65, 38, 66, 40, 67]).

In this context, scaling relations are very helpful to understand complex phenomena. [68], by fitting the rotation curves of 55 galaxies with a pseudo-isothermal profile, obtained some relations among the DM halos parameters.

They introduced the quantity $\Sigma = \mu_{0D} = \rho_0 r_0^1$, which behaves as a DMsd. According to their studies, for late type galaxies, $\Sigma = \mu_{0D} \simeq 100 M_\odot / pc^2$ independently from galaxy luminosity. This result has been studied and verified by several authors. [1] (D09), in agreement with [68], found again a quasi-universality of Σ , by analysing a set of 1000 galaxies (spirals, dwarfs, ellipticals, etc). Promptly, [2], showed that in MOND Σ , in the Newtonian regime, has a similar behavior to that described by D09, but noticed that in the case of galaxies having a low surface density Σ has a smaller value. Recently, [69] extended the work of [2] to spiral galaxies showing that for high baryon DMsd Σ is constant in agreement with [2], and D09, and for low baryon surface density Σ decreases.

From the literature is known that the Burkert profile gives good fits to LSBs, and dwarfs rotation curves ([70, 71, 38]. In the case of giant galaxies, and ellipticals the previous conclusion is not valid ([72, 73, 74, 72]).

Several authors obtained results in disagreement with those of D09.

By means of a much larger sample of that of D09 [75] showed that dark matter column density systematically increases with the mass of the halo. [76] showed that the column density, and the Newtonian acceleration, correlates with different quantities in agreement with [75], and in disagreement with D09 results.

In early-type galaxies, [77] did not find the existence of a universal DMsd.

¹ r_0 is the core radius of the pseudo-isothermal profile, and ρ_0 its central density

[78], in agreement with [77], [76], and [75], found signs of a correlation of DMsd with M_{200} .

[79] found a correlation between the Newtonian acceleration and the virial mass M_{vir} .

Several correlations between the surface density and a series of quantities are shown by [67], similarly to what found by [80]. In the last paper the DMsd was obtained by fitting the rotation curves of the galaxies with a Burkert profile, and using the Markov Chain Monte Carlo (MCMC) method to infer the values of the parameters.

In this paper, using SPARC's HSBs, and LSBs we want to study the behavior of the DMsd, to see whether it is either constant as claimed by D09, or it depends on the baryon surface density according to MOND. To this aim, we study the DMsd vs the magnitude and the baryon surface density in HSBs, and LSBs. HSBs shows a constant behavior of the DM, while LSBs shows that the behavior depends from the baryon surface density.

The paper is organized as follows. In Sect. 2, we introduce the SPARC sample and the analysis that was performed in a previous paper ([80]) to obtain the DMsd. In Sect. 3, we discuss the results, and Sect. 4 is devoted to discussion.

2. SPARC data set, and data analysis: a summary

In this section, we give a summary of the SPARC data used, and the analysis on the data, as performed by [80]. SPARC (*Spitzer* Photometry and Accurate Rotation Curves) dataset [81] is constituted by 175 late-type galaxies with high quality rotation curves obtained from HI/H α studies, and with surface photometry at 3.6 μm , giving the mass-to-light ratio Υ_* conversion factor. The gas mass is provided by 21 cm observations. Almost all SPARC galaxies have a disc structure, with some having also bulges. The baryon component is constituted by the disc, bulge, and gas components. The morphologies present in SPARC goes from SO to Irr. [80] obtained the DM surface density by fitting the rotation curves with a Burkert profile

$$\rho(r) = \frac{\rho_0 r_0^3}{(r + r_0)(r^2 + r_0^2)}, \quad (1)$$

where r_0 , and ρ_0 represent the scale radius and the central density of the halo, respectively.

The total rotational velocity is given by

$$V_{\text{tot}}^2 = V_{\text{DM}}^2 + V_{\text{bar}}^2 = V_{\text{DM}}^2 + \Upsilon_{\text{d}} V_{\text{disc}}^2 + \Upsilon_{\text{b}} V_{\text{bulge}}^2 + V_{\text{gas}}^2, \quad (2)$$

where V_{disc} , V_{bulge} , V_{gas} are the velocities of the baryonic component, and V_{DM} is that of the dark matter component, given by

$$\frac{V_{\text{DM}}^2}{V_{200}^2} = \frac{C_{200}}{x} \frac{\ln(1+x) + \frac{1}{2} \ln(1+x^2) - \arctan x}{\ln(1+C_{200}) + \frac{1}{2} \ln(1+C_{200}^2) - \arctan C_{200}}, \quad (3)$$

and the concentration C_{200} and the rotation velocity V_{200} at the virial radius r_{200} are given by

$$C_{200} = r_{200}/r_0, \quad V_{200} = 10C_{200}r_0H_0, \quad (4)$$

where H_0 is the Hubble constant (chosen to be $73 \text{ Km s}^{-1} \text{ Mpc}^{-1}$). The mass-to-light ratios for the disc and bulge component, are given by Υ_{d} , and Υ_{b} , respectively. An important point to recall is that the galaxy distance, and the disc inclination, affect the stellar components and the total observed rotational velocities, respectively. Then if the galaxy distance is changed from its value D to $D' = D\delta_{\text{D}}^2$, also the radius is affected and becomes $R' = R\delta_{\text{D}}$, and also the baryonic component velocity which becomes $V'_{\text{k}} = V_{\text{k}}\sqrt{\delta_{\text{D}}^3}$.

A change in disk inclination from i to $i' = i\delta_{\text{i}}^4$, produces a change in the observed rotation curves and their uncertainties, as

$$V'_{\text{obs}} = V_{\text{obs}} \frac{\sin(i)}{\sin(i')}, \quad \delta V'_{\text{obs}} = \delta V_{\text{obs}} \frac{\sin(i)}{\sin(i')}. \quad (5)$$

The observed rotational curve is fitted with a theoretical curve depending on several parameters: V_{200} , C_{200} , Υ_{d} , Υ_{b} , δ_{D} and δ_{i} . The calculation is performed through a Bayesian analysis. The posterior probability of parameter space is given by

$$P(V_{200}, C_{200}, \Upsilon_{\text{d}}, \Upsilon_{\text{b}}, \delta_{\text{D}}, \delta_{\text{i}} | \text{SPARC}) = \mathcal{L}(V_{200}, C_{200}, \Upsilon_{\text{d}}, \Upsilon_{\text{b}}, \delta_{\text{D}}, \delta_{\text{i}} | \text{SPARC}) P(V_{200}, C_{200}, \Upsilon_{\text{d}}, \Upsilon_{\text{b}}, \delta_{\text{D}}, \delta_{\text{i}}), \quad (6)$$

² δ_{D} is a dimensionless distance factor

³'k' denotes disc, bulge, or gas

⁴ δ_{i} is a dimensionless inclination factor

where the likelihood is obtained through $\mathcal{L} \sim e^{-\chi^2/2}$, and where χ^2 is given by

$$\chi^2 = \sum_{k=1}^N \left(\frac{V_{\text{tot}}(R'_k; V_{200}, C_{200}, \Upsilon_d, \Upsilon_b, \delta_D) - V'_{\text{obs},k}}{\delta V'_{\text{obs},k}} \right)^2, \quad (7)$$

In the previous relation, N is the number of data point for each galaxy, $V'_{\text{obs},k}$ and $\delta V'_{\text{obs},k}$ are the observed rotation curve and its uncertainty at the radius R'_k . The total rotation velocity V_{tot} at the radius R'_k depends on galactic parameters $\{\Upsilon_d, \Upsilon_b, \delta_D\}$, and halo parameters $\{V_{200}, C_{200}\}$. Since prior probabilities of parameters are uncorrelated it is given by

$$P(V_{200}, C_{200}, \Upsilon_d, \Upsilon_b, \delta_D, \delta_i) = P(V_{200})P(C_{200})P(\Upsilon_d)P(\Upsilon_b)P(\delta_D)P(\delta_i). \quad (8)$$

The priors on galactic parameters are set as in [82]: on δ_D and δ_i are imposed Gaussian priors around 1 with standard deviations given by the observational relative errors. On Υ_* is used a log-normal prior around their fiducial values $\Upsilon_d = 0.5$ and $\Upsilon_b = 0.7$ with a standard deviation of 0.1 dex. In the case of the halo parameters is used a flat prior with $10 < V_{200} < 500 \text{ km s}^{-1}$, $1 < C_{200} < 100$. Maximizing the posterior probability, one gets the best fitting value. The values of $\rho_0 r_0$, obtained with the previous method by [80], are in the second column of Table 1, while the values of the luminosity, and the effective surface brightness (taken from SPARC's webpage http://astroweb.cwru.edu/SPARC/SPARC_Lelli2016c.mrt) can be found in column 3, and 4 of Table 1, respectively.

As already reported, by means of the Bayesian method, [80] fitted 175 galaxy rotation curve of the SPARC sample. The fit to three representative galaxies has been shown in Fig. 1 of [80]. Burkert's profile gives a good fit to the galaxies studied. The galaxies studied, except five, have a reduced $\chi^2 < 10$, and the best fitting values and the reduced χ^2 for the SPARC sample are listed in Table 1 of [80].

3. Results

As discussed in the abstract, in this paper we have two goals. The first one is related to one claim of D09, namely that the DMsd is a constant universal quantity, equal to $\log(\Sigma/M_\odot \text{pc}^{-2}) = 2.15 \pm 0.2$. The second one, a MOND prediction, namely that

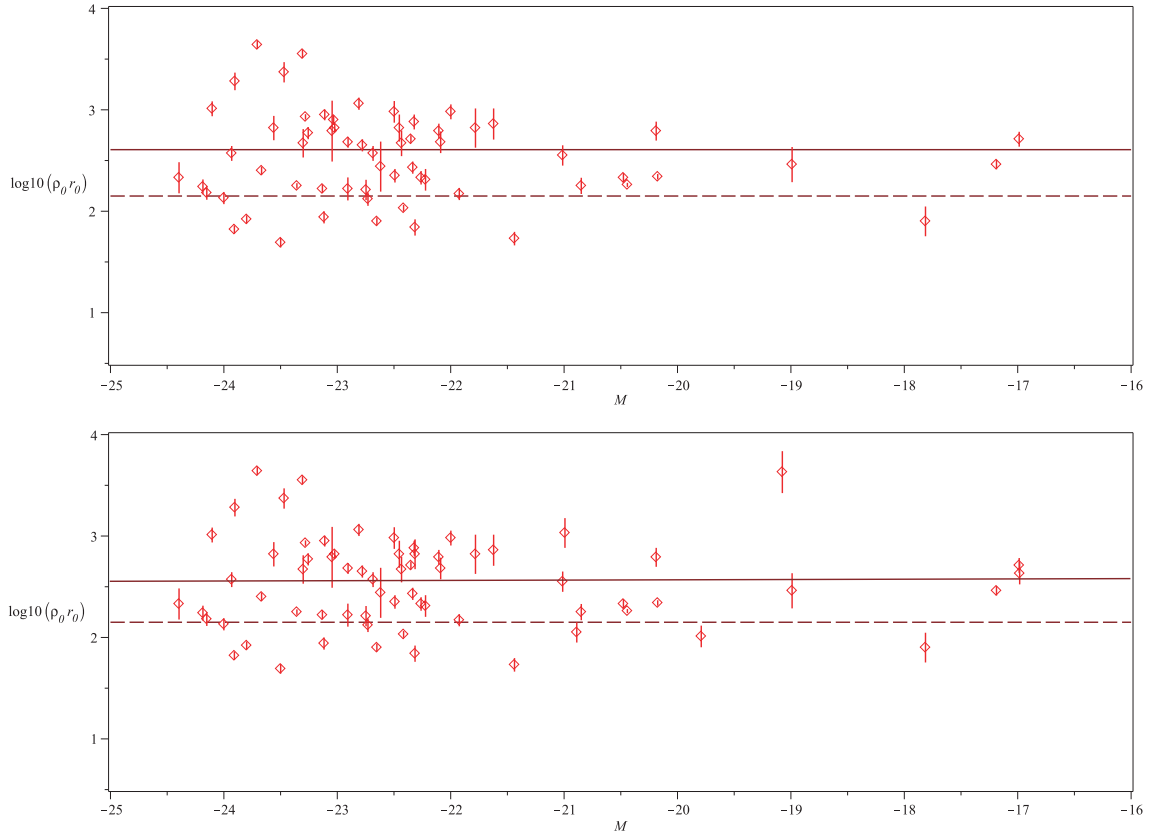


Figure 1: Upper panel: the DMsd in terms of the magnitude, M for HSBs. The data points with error-bars represent the HSBs with surface brightness larger than $300 L_{\odot}/\text{pc}^2$. The dashed line is the D09 value, and the solid line the fit to the data. Lower panel: same as the upper panel but for HSBs with surface brightness larger than $200 L_{\odot}/\text{pc}^2$.

for HSBs the DMsd is constant, and equal to $\log(\Sigma/M_{\odot}\text{pc}^{-2}) = 2.14$, while for LSBs the DMsd is not constant and has smaller values than for HSBs. At the first order the DMsd behaves as $\Sigma \simeq \sqrt{\Sigma_b \Sigma_M}$. In order to answer to these two questions, we used the SPARC (*Spitzer* Photometry and Accurate Rotation Curves) sample [81], constituted by 175 late-type galaxies with high quality rotation curves. We divided the sample in HSBs, and LSBs. In order to distinguish between these two classes of objects, we recall that the division between LSBs and HSBs is at $23 \text{ mag}/\text{arcsec}^2$ in B band. Recalling that in SPARC we have a photometry at $3.6 \mu\text{m}$, an estimate of

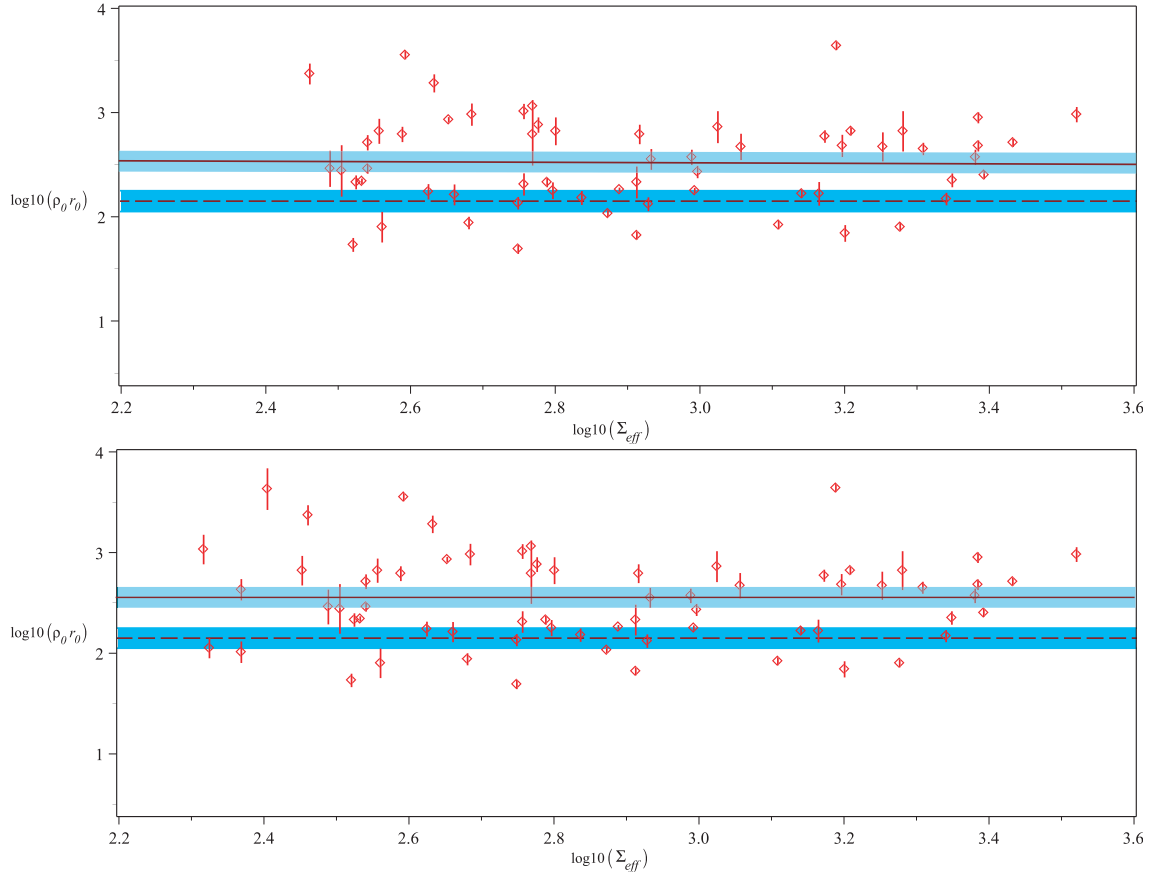


Figure 2: Upper panel: the DMsd in terms of the effective surface brightness, Σ_{eff} for HSBs. The data points with error-bars represent the HSBs with surface brightness larger than $300 L_{\odot}/\text{pc}^2$. The dashed line is the D09 value, the shaded region the 1σ confidence level region obtained using MOND, and the solid line the fit to the data. Lower panel: same as the upper panel but for HSBs with surface brightness larger than $200 L_{\odot}/\text{pc}^2$.

the threshold between LSBs and HSBs can be reasonably put at the effective surface brightness $\Sigma_{\text{eff}} = 200 L_{\odot}/\text{pc}^2$ (or $100 M_{\odot}/\text{pc}^2$ for $M/L = 0.5$)⁵.

In the paper, we consider several thresholds. For the HSBs, we use values of the effective surface brightness, $\Sigma_{\text{eff}}, > 200 L_{\odot}/\text{pc}^2$, and $> 300 L_{\odot}/\text{pc}^2$. For LSBs values

⁵Notice that the surface brightness distribution in SPARC is continuous even if the definition has a certain degree of arbitrariness

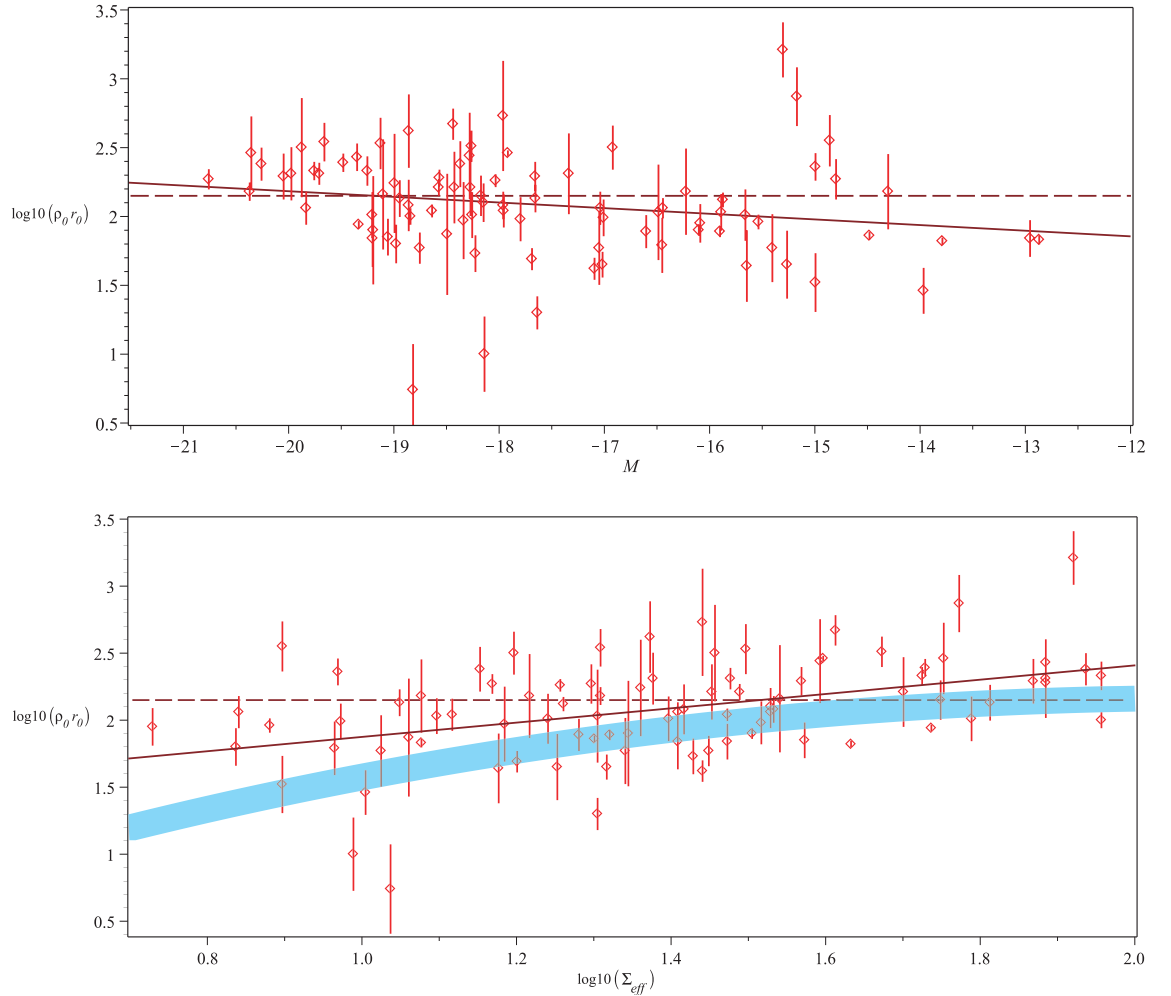


Figure 3: Upper panel: DMsd in terms of the magnitude, M for LSBs. The data points with error-bars represent the LSBs with surface brightness smaller than $100 L_{\odot}/\text{pc}^2$. The dashed line is the D09 value, and the solid line the fit to the data. Bottom panel: the DMsd in terms of the effective surface brightness, Σ_{eff} for LSBs with surface brightness smaller than $100 L_{\odot}/\text{pc}^2$. The dashed line is the D09 value, and the solid line the fit to the data. The shaded region the 1σ confidence level region obtained using MOND.

of $\Sigma_{\text{eff}} < 100L_{\odot}/\text{pc}^2$, and $\Sigma_{\text{eff}} < 25L_{\odot}/\text{pc}^2$. For a given value of M/L , the quoted threshold corresponds to thresholds in mass surface density M_{\odot}/pc^2 . The results are plotted in Figs. 1-4. In Fig. 1, we plot the DMsd in terms of the magnitude, M . The DMsd of the HSBs is represented by the data points with error-bars. The data points,

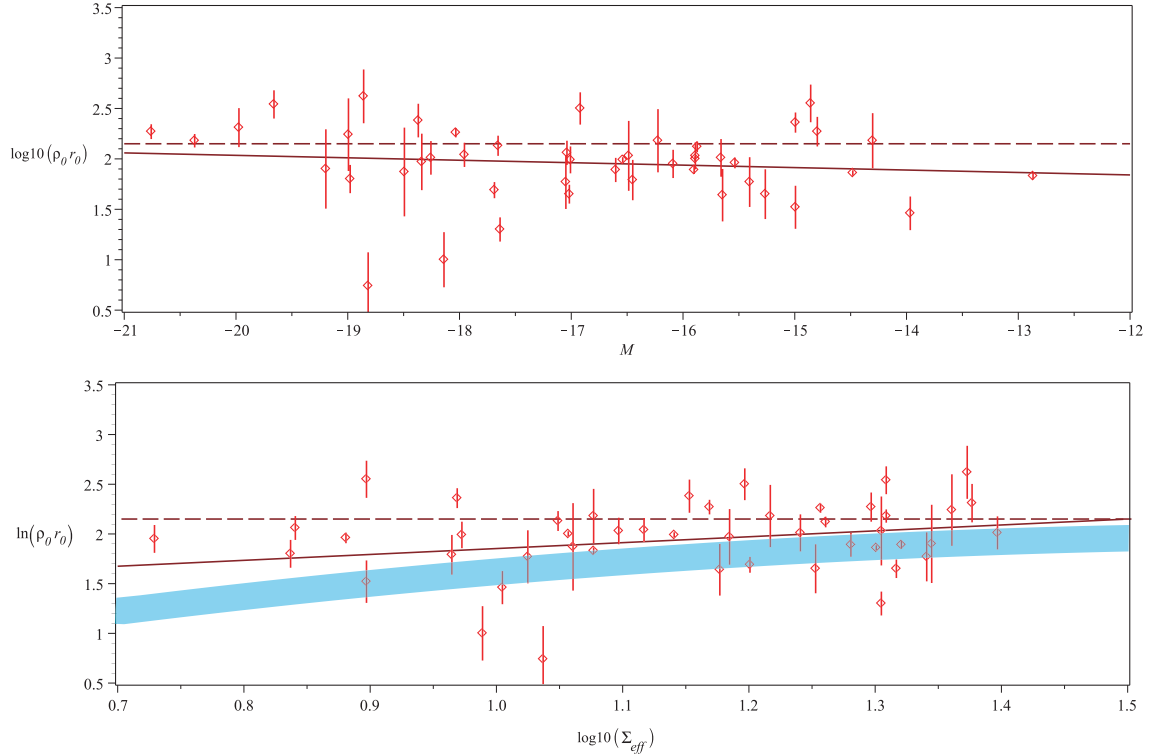


Figure 4: Same as Fig. 3 but for DMsd smaller than $25 L_{\odot}/\text{pc}^2$.

surface density of galaxies and errors, are obtained by [80] (Table A. 1). In the upper panel we used the galaxies (HSBs) with surface brightness $> 300 L_{\odot}/\text{pc}^2$. The lower panel represents the same quantities as the upper panel but in this case for HSBs with surface brightness larger than $200 L_{\odot}/\text{pc}^2$. In both panels, the dashed line is the D09 value, and the solid line the fit to the data. Both plots give the same information: the DMsd is constant, independent on the magnitude. This is qualitatively in agreement with D09, but the value of the constant DMsd is not $\log(\Sigma/M_{\odot}\text{pc}^{-2}) = 2.15 \pm 0.2$, but larger ($\log(\Sigma/M_{\odot}\text{pc}^{-2}) = 2.61$, for the upper panel). Another difference between D09 result and ours is that D09 claims that their result is valid for all kind of galaxies: LSBs, and HSBs. In reality, their conclusions is based on the analysis of dwarf spheroidal satellites of the Milky Way. They include only one well studied LSB: NGC 3741. In other terms their claim that their result can be applied to all galaxies

is not correct. The D09 result and our are in qualitative agreement because they are mainly using HSBs as we are doing in this first part of the analysis. Then HSBs are characterized by a constant DMsd. In Fig. 2, we plot the surface density in terms of the effective surface brightness, Σ_{eff} . As in Fig. 1, the data points with error-bars represent the HSBs with surface brightness larger than $300 L_{\odot}/\text{pc}^2$ (upper panel), and $200 L_{\odot}/\text{pc}^2$ (lower panel). The dashed line is the D09 value, and the solid line the fit to the data. We also plotted, as a shaded region, the 1σ confidence level region obtained using MOND (see Appendix). The plot gives two information: a) the DMsd is constant and does not depend on Σ_{eff} . b) MOND predicts a constant value of the DMsd equal to $\log(\Sigma/M_{\odot}\text{pc}^{-2}) = 2.14$ almost identical to that of D09, qualitatively in agreement with our result, for what concerns the constancy, but in disagreement with the value that we obtain, $\log(\Sigma/M_{\odot}\text{pc}^{-2}) = 2.54$ (upper panel). In Fig. 3, the upper panel represents the DMsd in terms of the magnitude, M . The data points with error-bars represent the LSBs with surface brightness smaller than $100 L_{\odot}/\text{pc}^2$. The dashed line is the D09 value, and the solid line the fit to the data. The plot shows that the DMsd decreases with increasing magnitude (smaller luminosity). However, in the range of magnitudes $\simeq -20.5$ to $\simeq -17.5$ the surface density, within the errors, is in agreement with a flat surface density close to that of D09. For smaller magnitudes several LSBs have a smaller value than that predicted by D09. In other terms, for $\Sigma_{\text{eff}} < 100L_{\odot}/\text{pc}^2$, for decreasing values of the magnitude the LSBs tend to have smaller values of the surface density with respect to D09. The bottom panel in Fig. 3, represents the DMsd in terms of Σ_{eff} . The behavior for decreasing values of Σ_{eff} is similar to that of the upper panel. Within the errors limits, and in the range $1.4 \preceq \log \Sigma_{\text{eff}} \preceq 2$, the DMsd is in agreement with the D09 result, after it has smaller values than D09. Still in the bottom panel it is also plotted a shaded region which is the 1σ confidence level region obtained using MOND. The plot shows that in the range $1.6 \preceq \log \Sigma_{\text{eff}} \preceq 2$, MOND is in agreement with D09 prediction, while for smaller values of Σ_{eff} it shows a decline towards smaller values of the surface density, in agreement with the data. The upper panel of Fig. 4, represents the surface density in terms of the magnitude, M . The data points with error-bars represent the LSBs with surface brightness smaller than $25 L_{\odot}/\text{pc}^2$. The trend with the magnitude of the DMsd is similar to that shown in Fig.

3, even if the values of the DMsd are smaller than that of D09 since the most negative magnitudes. The bottom panel in Fig. 4, represents the DMsd in terms of Σ_{eff} . As before the dots with error-bars represent the LSBs galaxies the shaded region is the 1σ confidence level region obtained using MOND, the solid line the fit to the LSBs with surface brightness smaller than $25 L_{\odot}/\text{pc}^2$, and the dashed line D09 prediction. Within the errors limits, and in the range $1.35 \lesssim \Sigma_{\text{eff}} \lesssim 1.5$, DMsd is in agreement with the D09 result, after it has smaller values than D09. The behavior for decreasing values of Σ_{eff} is similar to that of the upper panel. In this case MOND predicts a surface density smaller than that of D09 in the entire range of the data. As in Fig. 3, it shows a decline towards smaller values of the DMsd, in agreement with the data.

Summarizing the results till now reported, concerning HSBs, the DMsd is constant in terms of the magnitude (in qualitative agreement with D09) and Σ_{eff} (in qualitative agreement with MOND), but larger than the prediction of D09, and MOND. In the case of the LSBs, there is a decrease of the DMsd with the luminosity (in disagreement with D09), and a decrease of Σ_{eff} (in agreement with MOND), and it is usually smaller than the D09 prediction. MOND, is in qualitative agreement with the data predicts a decrease of the DMsd with Σ_{eff} .

4. Discussion

By means of the HSBs, and LSBs in SPARC we studied the DMsd of the class of galaxies in the sample. Our interest was that of understanding whether the DM surface density is a constant universal quantity equal to $\log(\Sigma/M_{\odot}\text{pc}^{-2}) = 2.15 \pm 0.2$, as claimed by D09 or if it assumes different classes of objects and their baryon surface density. At the same time, we studied the MOND prediction ([2, 69]), namely a constant DMsd in HSBs close to that predicted by D09, and a smaller, decreasing DMsd with decreasing surface brightness (baryon surface density) in the case of LSBs. In order to study these two issues, we grouped the SPARC sample in HSBs, and LSBs, and we also considered for these two groups of galaxies several thresholds in Σ_{eff} . In the case of HSBs, and for galaxies characterized by $\Sigma_{\text{eff}} > 200L_{\odot}/\text{pc}^2$, and $\Sigma_{\text{eff}} > 300L_{\odot}/\text{pc}^2$, we found that the DMsd vs magnitude is constant, as in D09,

and similarly, we found a constant DMsd vs Σ_{eff} as in MOND prediction. In spite of the fact that the result of our study, in the case of HSBs is in qualitative agreement with D09, and MOND, the value of the DMsd is larger than the one predicted by D09, and MOND. In the case of LSBs, we also used two thresholds: $\Sigma_{\text{eff}} < 100L_{\odot}/pc^2$, and $\Sigma_{\text{eff}} < 25L_{\odot}/pc^2$. For both thresholds, the DMsd is decreasing, with increasing value of magnitude (decreasing luminosity), in all magnitude range. In the case of $\Sigma_{\text{eff}} < 100L_{\odot}/pc^2$, the DMsd, within the errors, and in the range of magnitudes $\simeq -20.5$ to $\simeq -17.5$ is in agreement with a flat surface density close to that of D09. Going to smaller negative magnitudes several LSBs have a smaller value than that predicted by D09. In the case of LSBs with surface brightness smaller than $25L_{\odot}/pc^2$, the trend with magnitude of the surface density is similar to that of the previous case ($\Sigma_{\text{eff}} < 100L_{\odot}/pc^2$), even if the values of the DMsd are smaller than that of D09 since the most negative magnitudes. Concerning the trend of the DM surface density in terms of the Σ_{eff} for the two thresholds ($\Sigma_{\text{eff}} < 100L_{\odot}/pc^2$, and $\Sigma_{\text{eff}} < 25L_{\odot}/pc^2$), it is decreasing with decreasing Σ_{eff} . In the case $\Sigma_{\text{eff}} < 100L_{\odot}/pc^2$, the DMsd is, in the errors limits, and in the range $1.4 \preceq \log \Sigma_{\text{eff}} \preceq 2$, in agreement with the D09 result, after it has smaller values than D09. In the case $\Sigma_{\text{eff}} < 25L_{\odot}/pc^2$ the DMsd is, in the errors limits, and in the range $1.35 \preceq \Sigma_{\text{eff}} \preceq 1.5$, in agreement with the D09 result, after it has smaller values than D09. Concerning MOND's predictions, in the case $\Sigma_{\text{eff}} < 100L_{\odot}/pc^2$, and $1.6 \preceq \log \Sigma_{\text{eff}} \preceq 2$, MOND is in agreement with D09 prediction, while for smaller values of Σ_{eff} it shows a decline towards smaller values of the DMsd, in agreement with the data. In the case $\Sigma_{\text{eff}} < 25L_{\odot}/pc^2$, for all values of Σ_{eff} , DMsd is smaller than D09 prediction, and shows a decline towards smaller values of the DMsd, in agreement with data.

In summary, the SPARC's HSBs tell us that both D09, and MOND correctly predict a constant DMsd, even if the value predicted is smaller than that obtained from data. SPARC's LSBs shows a decrease of the DMsd with luminosity and surface brightness (or baryon surface density), in agreement with MOND but not with D09.

Appendix: DMsd in MOND

In this section, we summarize the calculation developed in [69] to obtain the DMsd in MOND. Using the MOND formulation by [83], the potential ϕ is given by a generalization of Poisson equation

$$\nabla[\mu(|\nabla\phi|/a_0)\nabla\phi] = 4\pi G\rho \quad (9)$$

where the baryon density is indicated by ρ , $\mu(x)$ is the interpolating function, and a_0 is the MOND constant. The difference between the MOND acceleration field $\nabla\phi$ and the Newtonian one, interpreted from a Newtonian point of view is explained by the presence of dark matter or as indicated by Milgrom, by "phantom matter" having a density [84]

$$\rho_P = \frac{1}{4\pi G}\Delta\phi - \rho \quad (10)$$

Using Eq. (9), we can write

$$\rho_P(\mathbf{r}) = -\frac{1}{4\pi G a_0} \frac{\mu'}{\mu} \nabla|\nabla\phi|\nabla\phi + \rho(\mathbf{r})(1/\mu - 1). \quad (11)$$

The previous equation can be written as

$$\rho_P = \rho_{P_1} + \rho_{P_2} = \frac{-a_0}{4\pi G} \mathbf{e} \cdot \nabla\mathcal{V}(|\nabla\phi|/a_0) + (1/\mu - 1)\rho. \quad (12)$$

After defining $\mathcal{V}(x) = \int L(x)dx$, $x = g/a_0$, $L = \frac{\mu'}{\mu}x$, and defining a vector \mathbf{e} in the direction of $\nabla\phi$, we also have

$$\rho_P = \rho_{P_1} + \rho_{P_2} = \frac{-a_0}{4\pi G} \mathbf{e} \cdot \nabla\mathcal{V}(|\nabla\phi|/a_0) + (1/\mu - 1)\rho, \quad (13)$$

with

$$\rho_{P_1} = \frac{-a_0}{4\pi G} \mathbf{e} \cdot \nabla\mathcal{V}(|\nabla\phi|/a_0), \quad (14)$$

$$\rho_{P_2} = (1/\mu - 1)\rho. \quad (15)$$

The integral of Equation (13) is calculated considering two cases: $x \geq 1$ (acceleration above the MOND universal constant), and $x \leq 1$. Let us consider the second term (Equation 15), $\rho_{P_2} = (1/\mu - 1)\rho$. We write $a_N = \frac{g_N}{a_0} = (g/a_0)\mu(g/a_0)$, where $g_N = g\mu(g/a_0)$ is the Newtonian acceleration.

In the case $n = 1$, and $\mu = \frac{x}{(1+x^n)^{1/n}} = \frac{g/a_0}{1+g/a_0}$, multiplying for μ we have

$$\mu = \frac{\mu g/a_0}{\mu g/a_0 + \mu} = \frac{a_N}{a_N + \mu}, \quad (16)$$

solving with respect to μ we have

$$\mu = -1/2a_N + 1/2\sqrt{a_N^2 + 4a_N}. \quad (17)$$

For a double exponential disk, with cylindrical radius R and altitude z , we have

$$a_N \simeq \frac{GM}{a_0 R^2} = \frac{G2\pi\rho_0 h_z h_r^2}{a_0 R^2} \simeq \frac{\Sigma_b}{\Sigma_M} \frac{h_r^2}{R^2} \quad (18)$$

being Σ_b , the baryonic surface density, approximated by an integrated constant volume density ($\Sigma_b \simeq \int \rho_0 dz = \rho_0 h_z$).

The MOND interpolating function becomes

$$\mu = -1/2 \frac{\Sigma_b h_r^2}{\Sigma_M R^2} + 1/2 \sqrt{\frac{\Sigma_b^2 h_r^4}{\Sigma_M^2 R^4} + 4 \frac{\Sigma_b h_r^2}{\Sigma_M R^2}}. \quad (19)$$

Then

$$\frac{1-\mu}{\mu} \int_{-\infty}^{+\infty} \rho dz = 2(1-\mu)x\Sigma_M \frac{R^2}{h_r^2} \exp^{-R/h_r}. \quad (20)$$

The integral of the first (Eq. 13) term is given by

$$\begin{aligned} \int_{-\infty}^{+\infty} \rho_{P_1} dz &= 2 \int_0^{\infty} \rho_{P_1} dz = \\ &= \Sigma_M [\mathcal{V}(\infty) - \mathcal{V}(0)] = \\ &= \Sigma_M \int_0^{\infty} L(x) dx = a\Sigma_M, \end{aligned} \quad (21)$$

where $\Sigma_M = \frac{a_0}{2\pi G}$.

Integrating the Burkert profile D09 obtained a surface density given by

$$\Sigma_0 = 2 \int \rho dr = 2 \int \frac{\rho_0 r_0^3}{(r+r_0)(r^2+r_0^2)} = \frac{\pi}{2} \rho_0 r_0 = \frac{\pi}{2} \Sigma_c. \quad (22)$$

If we call Σ_c^* the MOND analog of Σ_c we have

$$\Sigma_c^* = \frac{2\lambda}{\pi} \Sigma_M, \quad (23)$$

with $\Sigma_M = 138 \frac{a_0}{1.2 \times 10^{-8} \text{cms}^{-2}} M_{\odot} / \text{pc}^2$.

The full integral can be written as

$$F = F_1 + F_2 = \frac{2}{\pi} \Sigma_M \int_0^x L(x) dx + \frac{2}{\pi} 2(1 - \mu) x \Sigma_M \frac{R^2}{h_r^2} \exp^{-R/h_r}. \quad (24)$$

As shown in [69], in the case $x \leq 1$ we have

$$\begin{aligned} F &= \frac{2}{\pi} \Sigma_M \arctan\left(\sqrt{\frac{\Sigma_b}{\Sigma_M}} \frac{h_r}{R}\right) + \\ &\frac{2}{\pi} 2 \frac{R \Sigma_M}{h_r} \left(1 + 1/2 \frac{\Sigma_b h_r^2}{\Sigma_M R^2} - 1/2 \sqrt{\frac{\Sigma_b^2 h_r^4}{\Sigma_M^2 R^4} + 4 \frac{\Sigma_b h_r^2}{\Sigma_M R^2}}\right) \\ &\times \sqrt{\frac{\Sigma_b}{\Sigma_M}} e^{-\frac{R}{h_r}}. \end{aligned} \quad (25)$$

At small x the first term in the right hand side tend to zero, and F is dominated by the second term. At first order the trend of F is $\sqrt{\Sigma_b \Sigma_M}$.

In the case $x \geq 1$, we have

$$\begin{aligned} F &= \frac{2}{\pi} \Sigma_M \arctan\left(\frac{\Sigma_b}{\Sigma_M} \frac{h_r^2}{R^2}\right) + \\ &\frac{4}{\pi} \left(1 + 1/2 \frac{\Sigma_b h_r^2}{\Sigma_M R^2} - 1/2 \sqrt{\frac{\Sigma_b^2 h_r^4}{\Sigma_M^2 R^4} + 4 \frac{\Sigma_b h_r^2}{\Sigma_M R^2}}\right) \\ &\times \Sigma_M e^{-\frac{R}{h_r}} R^2 / h_r^2. \end{aligned} \quad (26)$$

For large x , the second term tends to 0, $O(1)$, and the first one is $\simeq \Sigma_M$.

As it comes from the previous results and the plots in [69] there is a double trend of the surface density. For $R = h_r$, and at small Σ_b/Σ_M , the surface density increases as $\sqrt{\frac{\Sigma_b}{\Sigma_M}} \Sigma_M$. For larger Σ_b/Σ_M , the behavior of the surface density flattens till when, at large Σ_b/Σ_M tends to Σ_M .

Acknowledgements

The author thanks Valerio Pirronello for a careful reading of the manuscript. Financial contribution from the Programma ricerca di Ateneo UNICT 2020-22 linea 2 is graciously acknowledged. All authors read and approved the final manuscript.

References

- [1] F. Donato, G. Gentile, P. Salucci, C. Frigerio Martins, M. I. Wilkinson, G. Gilmore, E. K. Grebel, A. Koch, R. Wyse, A constant dark matter halo surface density in galaxies, *MNRAS*397 (2009) 1169–1176. [arXiv:0904.4054](#), [doi:10.1111/j.1365-2966.2009.15004.x](#).
- [2] M. Milgrom, The central surface density of ‘dark haloes’ predicted by MOND, *MNRAS*398 (2) (2009) 1023–1026. [arXiv:0909.5184](#), [doi:10.1111/j.1365-2966.2009.15255.x](#).
- [3] D. N. Spergel, L. Verde, H. V. Peiris, E. Komatsu, M. R. Nolta, C. L. Bennett, M. Halpern, G. Hinshaw, N. Jarosik, A. Kogut, M. Limon, S. S. Meyer, L. Page, G. S. Tucker, J. L. Weiland, E. Wollack, E. L. Wright, First-Year Wilkinson Microwave Anisotropy Probe (WMAP) Observations: Determination of Cosmological Parameters, *ApJS*148 (2003) 175–194. [arXiv:astro-ph/0302209](#), [doi:10.1086/377226](#).
- [4] M. Kowalski, D. Rubin, G. Aldering, R. J. Agostinho, A. Amadon, R. Amanullah, C. Balland, K. Barbary, G. Blanc, P. J. Challis, A. Conley, e. a. Connolly, N. V., Improved Cosmological Constraints from New, Old, and Combined Supernova Data Sets, *ApJ*686 (2008) 749–778. [arXiv:0804.4142](#), [doi:10.1086/589937](#).
- [5] W. J. Percival, B. A. Reid, D. J. Eisenstein, N. A. Bahcall, T. Budavari, J. A. Frieman, M. Fukugita, J. E. Gunn, e. a. Ivezić, Ž., Baryon acoustic oscillations in the Sloan Digital Sky Survey Data Release 7 galaxy sample, *MNRAS*401 (2010) 2148–2168. [arXiv:0907.1660](#), [doi:10.1111/j.1365-2966.2009.15812.x](#).
- [6] E. Komatsu, K. M. Smith, J. Dunkley, C. L. Bennett, B. Gold, G. Hinshaw, N. Jarosik, D. Larson, M. R. Nolta, L. Page, Seven-year Wilkinson Microwave Anisotropy Probe (WMAP) Observations: Cosmological Interpretation, *ApJS*192 (2) (2011) 18. [arXiv:1001.4538](#), [doi:10.1088/0067-0049/192/2/18](#).

- [7] A. Del Popolo, Dark matter, density perturbations, and structure formation, *Astronomy Reports* 51 (3) (2007) 169–196. [arXiv:0801.1091](#), [doi:10.1134/S1063772907030018](#).
- [8] A. Del Popolo, Non-baryonic dark matter in cosmology 1548 (2013) 2–63. [doi:10.1063/1.4817029](#).
- [9] A. Del Popolo, Nonbaryonic Dark Matter in Cosmology, *International Journal of Modern Physics D* 23 (2014) 30005. [arXiv:1305.0456](#), [doi:10.1142/S0218271814300055](#).
- [10] S. Weinberg, The cosmological constant problem, *Reviews of Modern Physics* 61 (1989) 1–23. [doi:10.1103/RevModPhys.61.1](#).
- [11] A. V. Astashenok, A. del Popolo, Cosmological measure with volume averaging and the vacuum energy problem, *Classical and Quantum Gravity* 29 (8) (2012) 085014. [arXiv:1203.2290](#), [doi:10.1088/0264-9381/29/8/085014](#).
- [12] H. E. S. Velten, R. F. vom Marttens, W. Zimdahl, Aspects of the cosmological “coincidence problem”, *European Physical Journal C* 74 (2014) 3160. [arXiv:1410.2509](#), [doi:10.1140/epjc/s10052-014-3160-4](#).
- [13] E. Di Valentino, O. Mena, S. Pan, L. Visinelli, W. Yang, A. Melchiorri, D. F. Mota, A. G. Riess, J. Silk, In the realm of the Hubble tension—a review of solutions, *Classical and Quantum Gravity* 38 (15) (2021) 153001. [arXiv:2103.01183](#), [doi:10.1088/1361-6382/ac086d](#).
- [14] E. Macaulay, I. K. Wehus, H. K. Eriksen, Lower Growth Rate from Recent Redshift Space Distortion Measurements than Expected from Planck, *Physical Review Letters* 111 (16) (2013) 161301. [arXiv:1303.6583](#), [doi:10.1103/PhysRevLett.111.161301](#).
- [15] M. Raveri, Is there concordance within the concordance Λ CDM model?, *ArXiv e-prints* (Oct. 2015). [arXiv:1510.00688](#).

- [16] H. K. Eriksen, F. K. Hansen, A. J. Banday, K. M. Górski, P. B. Lilje, Asymmetries in the Cosmic Microwave Background Anisotropy Field, *ApJ*605 (2004) 14–20. [arXiv:astro-ph/0307507](#), [doi:10.1086/382267](#).
- [17] F. K. Hansen, A. J. Banday, K. M. Górski, Testing the cosmological principle of isotropy: local power-spectrum estimates of the WMAP data, *MNRAS*354 (2004) 641–665. [arXiv:astro-ph/0404206](#), [doi:10.1111/j.1365-2966.2004.08229.x](#).
- [18] T. R. Jaffe, A. J. Banday, H. K. Eriksen, K. M. Górski, F. K. Hansen, Evidence of Vorticity and Shear at Large Angular Scales in the WMAP Data: A Violation of Cosmological Isotropy?, *ApJL*629 (2005) L1–L4. [arXiv:astro-ph/0503213](#), [doi:10.1086/444454](#).
- [19] J. Hoftuft, H. K. Eriksen, A. J. Banday, K. M. Górski, F. K. Hansen, P. B. Lilje, Increasing Evidence for Hemispherical Power Asymmetry in the Five-Year WMAP Data, *ApJ*699 (2009) 985–989. [arXiv:0903.1229](#), [doi:10.1088/0004-637X/699/2/985](#).
- [20] Planck Collaboration, P. A. R. Ade, N. Aghanim, C. Armitage-Caplan, M. Arnaud, M. Ashdown, F. Atrio-Barandela, J. Aumont, C. Baccigalupi, A. J. Banday, et al., Planck 2013 results. XXIII. Isotropy and statistics of the CMB, *A&A*571 (2014) A23. [arXiv:1303.5083](#), [doi:10.1051/0004-6361/201321534](#).
- [21] Y. Akrami, Y. Fantaye, A. Shafieloo, H. K. Eriksen, F. K. Hansen, A. J. Banday, K. M. Górski, Power Asymmetry in WMAP and Planck Temperature Sky Maps as Measured by a Local Variance Estimator, *ApJL*784 (2014) L42. [arXiv:1402.0870](#), [doi:10.1088/2041-8205/784/2/L42](#).
- [22] D. J. Schwarz, G. D. Starkman, D. Huterer, C. J. Copi, Is the Low- l Microwave Background Cosmic?, *Physical Review Letters* 93 (22) (2004) 221301. [arXiv:astro-ph/0403353](#), [doi:10.1103/PhysRevLett.93.221301](#).

- [23] C. J. Copi, D. Huterer, D. J. Schwarz, G. D. Starkman, On the large-angle anomalies of the microwave sky, *MNRAS*367 (2006) 79–102. [arXiv:astro-ph/0508047](https://arxiv.org/abs/astro-ph/0508047), [doi:10.1111/j.1365-2966.2005.09980.x](https://doi.org/10.1111/j.1365-2966.2005.09980.x).
- [24] C. J. Copi, D. Huterer, D. J. Schwarz, G. D. Starkman, Uncorrelated universe: Statistical anisotropy and the vanishing angular correlation function in WMAP years 1–3, *Physical Review D*75 (2) (2007) 023507. [arXiv:astro-ph/0605135](https://arxiv.org/abs/astro-ph/0605135), [doi:10.1103/PhysRevD.75.023507](https://doi.org/10.1103/PhysRevD.75.023507).
- [25] C. J. Copi, D. Huterer, D. J. Schwarz, G. D. Starkman, Large-Angle Anomalies in the CMB, *Advances in Astronomy* 2010 (2010) 847541. [arXiv:1004.5602](https://arxiv.org/abs/1004.5602), [doi:10.1155/2010/847541](https://doi.org/10.1155/2010/847541).
- [26] C. J. Copi, D. Huterer, D. J. Schwarz, G. D. Starkman, Large-scale alignments from WMAP and Planck, *MNRAS*449 (2015) 3458–3470. [arXiv:1311.4562](https://arxiv.org/abs/1311.4562), [doi:10.1093/mnras/stv501](https://doi.org/10.1093/mnras/stv501).
- [27] M. Cruz, E. Martínez-González, P. Vielva, L. Cayón, Detection of a non-Gaussian spot in WMAP, *MNRAS*356 (2005) 29–40. [arXiv:astro-ph/0405341](https://arxiv.org/abs/astro-ph/0405341), [doi:10.1111/j.1365-2966.2004.08419.x](https://doi.org/10.1111/j.1365-2966.2004.08419.x).
- [28] M. Cruz, M. Tucci, E. Martínez-González, P. Vielva, The non-Gaussian cold spot in Wilkinson Microwave Anisotropy Probe: significance, morphology and foreground contribution, *MNRAS*369 (2006) 57–67. [arXiv:astro-ph/0601427](https://arxiv.org/abs/astro-ph/0601427), [doi:10.1111/j.1365-2966.2006.10312.x](https://doi.org/10.1111/j.1365-2966.2006.10312.x).
- [29] M. Cruz, L. Cayón, E. Martínez-González, P. Vielva, J. Jin, The Non-Gaussian Cold Spot in the 3 Year Wilkinson Microwave Anisotropy Probe Data, *ApJ*655 (2007) 11–20. [arXiv:astro-ph/0603859](https://arxiv.org/abs/astro-ph/0603859), [doi:10.1086/509703](https://doi.org/10.1086/509703).
- [30] J. F. Navarro, C. S. Frenk, S. D. M. White, The Structure of Cold Dark Matter Halos, *ApJ*462 (1996) 563. [arXiv:astro-ph/9508025](https://arxiv.org/abs/astro-ph/9508025), [doi:10.1086/177173](https://doi.org/10.1086/177173).

- [31] J. F. Navarro, C. S. Frenk, S. D. M. White, A Universal Density Profile from Hierarchical Clustering, *ApJ*490 (1997) 493. [arXiv:astro-ph/9611107](#), [doi:10.1086/304888](#).
- [32] J. F. Navarro, A. Ludlow, V. Springel, J. Wang, M. Vogelsberger, S. D. M. White, A. Jenkins, C. S. Frenk, A. Helmi, The diversity and similarity of simulated cold dark matter haloes, *MNRAS*402 (2010) 21–34. [arXiv:0810.1522](#), [doi:10.1111/j.1365-2966.2009.15878.x](#).
- [33] B. Moore, Evidence against dissipation-less dark matter from observations of galaxy haloes, *Nature*370 (1994) 629–631. [doi:10.1038/370629a0](#).
- [34] R. A. Flores, J. R. Primack, Observational and theoretical constraints on singular dark matter halos, *ApJL*427 (1994) L1–L4. [arXiv:astro-ph/9402004](#), [doi:10.1086/187350](#).
- [35] A. Burkert, The Structure of Dark Matter Halos in Dwarf Galaxies, *ApJL*447 (1995) L25. [arXiv:astro-ph/9504041](#), [doi:10.1086/309560](#).
- [36] W. J. G. de Blok, A. Bosma, S. McGaugh, Simulating observations of dark matter dominated galaxies: towards the optimal halo profile, *MNRAS*340 (2003) 657–678. [arXiv:astro-ph/0212102](#), [doi:10.1046/j.1365-8711.2003.06330.x](#).
- [37] R. A. Swaters, B. F. Madore, F. C. van den Bosch, M. Balcells, The Central Mass Distribution in Dwarf and Low Surface Brightness Galaxies, *ApJ*583 (2003) 732–751. [arXiv:astro-ph/0210152](#), [doi:10.1086/345426](#).
- [38] A. Del Popolo, The Cusp/Core Problem and the Secondary Infall Model, *ApJ*698 (2009) 2093–2113. [arXiv:0906.4447](#), [doi:10.1088/0004-637X/698/2/2093](#).
- [39] A. Del Popolo, P. Kroupa, Density profiles of dark matter haloes on galactic and cluster scales, *A&A*502 (2009) 733–747. [arXiv:0906.1146](#), [doi:10.1051/0004-6361/200811404](#).

- [40] A. Del Popolo, Density profile slopes of dwarf galaxies and their environment, *MNRAS*419 (2012) 971–984. [arXiv:1105.0090](#), [doi:10.1111/j.1365-2966.2011.19754.x](#).
- [41] A. Del Popolo, N. Hiotelis, Cusps and cores in the presence of galactic bulges, *JCAP*1 (2014) 47. [arXiv:1401.6577](#), [doi:10.1088/1475-7516/2014/01/047](#).
- [42] A. Klypin, A. V. Kravtsov, O. Valenzuela, F. Prada, Where Are the Missing Galactic Satellites?, *ApJ*522 (1999) 82–92. [arXiv:astro-ph/9901240](#), [doi:10.1086/307643](#).
- [43] B. Moore, T. Quinn, F. Governato, J. Stadel, G. Lake, Cold collapse and the core catastrophe, *MNRAS*310 (1999) 1147–1152. [arXiv:astro-ph/9903164](#), [doi:10.1046/j.1365-8711.1999.03039.x](#).
- [44] S. Garrison-Kimmel, M. Rocha, M. Boylan-Kolchin, J. S. Bullock, J. Lally, Can feedback solve the too-big-to-fail problem?, *MNRAS*433 (4) (2013) 3539–3546. [arXiv:1301.3137](#), [doi:10.1093/mnras/stt984](#).
- [45] S. Garrison-Kimmel, M. Boylan-Kolchin, J. S. Bullock, E. N. Kirby, Too big to fail in the Local Group, *MNRAS*444 (1) (2014) 222–236. [arXiv:1404.5313](#), [doi:10.1093/mnras/stu1477](#).
- [46] M. S. Pawlowski, B. Famaey, H. Jerjen, D. Merritt, P. Kroupa, J. Dabringhausen, F. Lüghausen, D. A. Forbes, G. Hensler, F. Hammer, M. Puech, S. Fouquet, H. Flores, Y. Yang, Co-orbiting satellite galaxy structures are still in conflict with the distribution of primordial dwarf galaxies, *MNRAS*442 (2014) 2362–2380. [arXiv:1406.1799](#), [doi:10.1093/mnras/stu1005](#).
- [47] T. Sawala, M. Cautun, C. Frenk, J. Helly, J. Jasche, A. Jenkins, P. H. Johansson, G. Lavaux, S. McAlpine, M. Schaller, The Milky Way’s plane of satellites is consistent with Λ CDM, *Nature Astronomy* (Dec. 2022). [arXiv:2205.02860](#), [doi:10.1038/s41550-022-01856-z](#).

- [48] A. R. Zentner, J. S. Bullock, Halo Substructure and the Power Spectrum, *ApJ*598 (2003) 49–72. [arXiv:astro-ph/0304292](#), [doi:10.1086/378797](#).
- [49] P. Colín, V. Avila-Reese, O. Valenzuela, Substructure and Halo Density Profiles in a Warm Dark Matter Cosmology, *ApJ*542 (2000) 622–630. [arXiv:astro-ph/0004115](#), [doi:10.1086/317057](#).
- [50] J. Sommer-Larsen, A. Dolgov, Formation of Disk Galaxies: Warm Dark Matter and the Angular Momentum Problem, *ApJ*551 (2001) 608–623. [arXiv:astro-ph/9912166](#), [doi:10.1086/320211](#).
- [51] J. Goodman, Repulsive dark matter, *New Astronomy*5 (2000) 103–107. [arXiv:astro-ph/0003018](#), [doi:10.1016/S1384-1076\(00\)00015-4](#).
- [52] P. J. E. Peebles, Fluid Dark Matter, *ApJL*534 (2000) L127–L129. [arXiv:astro-ph/0002495](#), [doi:10.1086/312677](#).
- [53] H. A. Buchdahl, Non-linear Lagrangians and cosmological theory, *MNRAS*150 (1970) 1.
- [54] A. A. Starobinsky, A new type of isotropic cosmological models without singularity, *Physics Letters B* 91 (1980) 99–102. [doi:10.1016/0370-2693\(80\)90670-X](#).
- [55] M. Milgrom, A modification of the Newtonian dynamics as a possible alternative to the hidden mass hypothesis, *ApJ*270 (1983) 365–370. [doi:10.1086/161130](#).
- [56] M. Milgrom, A modification of the Newtonian dynamics - Implications for galaxies, *ApJ*270 (1983) 371–389. [doi:10.1086/161131](#).
- [57] R. Ferraro, $f(R)$ and $f(T)$ theories of modified gravity 1471 (2012) 103–110. [arXiv:1204.6273](#), [doi:10.1063/1.4756821](#).
- [58] J. F. Navarro, V. R. Eke, C. S. Frenk, The cores of dwarf galaxy haloes, *MNRAS*283 (1996) L72–L78. [arXiv:astro-ph/9610187](#).

- [59] S. Gelato, J. Sommer-Larsen, On DDO 154 and cold dark matter halo profiles, *MNRAS*303 (1999) 321–328. [arXiv:astro-ph/9806289](https://arxiv.org/abs/astro-ph/9806289), [doi:10.1046/j.1365-8711.1999.02223.x](https://doi.org/10.1046/j.1365-8711.1999.02223.x).
- [60] J. I. Read, G. Gilmore, Mass loss from dwarf spheroidal galaxies: the origins of shallow dark matter cores and exponential surface brightness profiles, *MNRAS*356 (2005) 107–124. [arXiv:astro-ph/0409565](https://arxiv.org/abs/astro-ph/0409565), [doi:10.1111/j.1365-2966.2004.08424.x](https://doi.org/10.1111/j.1365-2966.2004.08424.x).
- [61] S. Mashchenko, H. M. P. Couchman, J. Wadsley, The removal of cusps from galaxy centres by stellar feedback in the early Universe, *Nature*442 (2006) 539–542. [arXiv:astro-ph/0605672](https://arxiv.org/abs/astro-ph/0605672), [doi:10.1038/nature04944](https://doi.org/10.1038/nature04944).
- [62] F. Governato, C. Brook, L. Mayer, A. Brooks, G. Rhee, J. Wadsley, P. Jonsson, B. Willman, G. Stinson, T. Quinn, P. Madau, Bulgeless dwarf galaxies and dark matter cores from supernova-driven outflows, *Nature*463 (2010) 203–206. [arXiv:0911.2237](https://arxiv.org/abs/0911.2237), [doi:10.1038/nature08640](https://doi.org/10.1038/nature08640).
- [63] A. El-Zant, I. Shlosman, Y. Hoffman, Dark Halos: The Flattening of the Density Cusp by Dynamical Friction, *ApJ*560 (2001) 636–643. [arXiv:astro-ph/0103386](https://arxiv.org/abs/astro-ph/0103386), [doi:10.1086/322516](https://doi.org/10.1086/322516).
- [64] A. A. El-Zant, Y. Hoffman, J. Primack, F. Combes, I. Shlosman, Flat-cored Dark Matter in Cuspy Clusters of Galaxies, *ApJL*607 (2004) L75–L78. [arXiv:astro-ph/0309412](https://arxiv.org/abs/astro-ph/0309412), [doi:10.1086/421938](https://doi.org/10.1086/421938).
- [65] E. Romano-Díaz, I. Shlosman, Y. Hoffman, C. Heller, Erasing Dark Matter Cusps in Cosmological Galactic Halos with Baryons, *ApJL*685 (2008) L105–L108. [arXiv:0808.0195](https://arxiv.org/abs/0808.0195), [doi:10.1086/592687](https://doi.org/10.1086/592687).
- [66] D. R. Cole, W. Dehnen, M. I. Wilkinson, Weakening dark matter cusps by clumpy baryonic infall, *MNRAS*416 (2011) 1118–1134. [arXiv:1105.4050](https://arxiv.org/abs/1105.4050), [doi:10.1111/j.1365-2966.2011.19110.x](https://doi.org/10.1111/j.1365-2966.2011.19110.x).

- [67] A. Saburova, A. Del Popolo, On the surface density of dark matter haloes, *MNRAS*445 (4) (2014) 3512–3524. [arXiv:1410.3052](#), [doi:10.1093/mnras/stu1957](#).
- [68] J. Kormendy, K. C. Freeman, Scaling Laws for Dark Matter Halos in Late-Type and Dwarf Spheroidal Galaxies 220 (2004) 377. [arXiv:astro-ph/0407321](#).
- [69] A. Del Popolo, M. Le Delliou, Surface Density of Disk Galaxies in MOND, *Universe* 9 (1) (2023) 32. [doi:10.3390/universe9010032](#).
- [70] G. Gentile, P. Salucci, U. Klein, D. Vergani, P. Kalberla, The cored distribution of dark matter in spiral galaxies, *MNRAS*351 (2004) 903–922. [arXiv:astro-ph/0403154](#), [doi:10.1111/j.1365-2966.2004.07836.x](#).
- [71] G. Gentile, P. Salucci, U. Klein, G. L. Granato, NGC 3741: the dark halo profile from the most extended rotation curve, *MNRAS*375 (2007) 199–212. [arXiv:astro-ph/0611355](#), [doi:10.1111/j.1365-2966.2006.11283.x](#).
- [72] J. D. Simon, A. D. Bolatto, A. Leroy, L. Blitz, E. L. Gates, High-Resolution Measurements of the Halos of Four Dark Matter-Dominated Galaxies: Deviations from a Universal Density Profile, *ApJ*621 (2005) 757–776. [arXiv:astro-ph/0412035](#), [doi:10.1086/427684](#).
- [73] W. J. G. de Blok, F. Walter, E. Brinks, C. Trachternach, S.-H. Oh, R. C. Kennicutt, Jr., High-Resolution Rotation Curves and Galaxy Mass Models from THINGS, *AJ*136 (2008) 2648–2719. [arXiv:0810.2100](#), [doi:10.1088/0004-6256/136/6/2648](#).
- [74] A. Del Popolo, On the density-profile slope of clusters of galaxies, *MNRAS*424 (2012) 38–51. [arXiv:1204.4439](#), [doi:10.1111/j.1365-2966.2012.21141.x](#).

- [75] A. Boyarsky, O. Ruchayskiy, D. Iakubovskiy, A. V. Maccio', D. Malyshev, New evidence for dark matter, ArXiv e-prints (Nov. 2009). [arXiv:0911.1774](#).
- [76] V. F. Cardone, C. Tortora, Dark matter scaling relations in intermediate z haloes, MNRAS409 (2010) 1570–1576. [arXiv:1007.3673](#), [doi:10.1111/j.1365-2966.2010.17398.x](#).
- [77] N. R. Napolitano, A. J. Romanowsky, C. Tortora, The central dark matter content of early-type galaxies: scaling relations and connections with star formation histories, MNRAS405 (2010) 2351–2371. [arXiv:1003.1716](#), [doi:10.1111/j.1365-2966.2010.16710.x](#).
- [78] A. Del Popolo, V. F. Cardone, G. Belvedere, Surface density of dark matter haloes on galactic and cluster scales, MNRAS429 (2013) 1080–1087. [arXiv:1212.6797](#), [doi:10.1093/mnras/sts389](#).
- [79] V. F. Cardone, A. Del Popolo, Newtonian acceleration scales in spiral galaxies, MNRAS427 (2012) 3176–3187. [arXiv:1209.1524](#), [doi:10.1111/j.1365-2966.2012.21982.x](#).
- [80] Y. Zhou, A. Del Popolo, Z. Chang, On the absence of a universal surface density, and a maximum Newtonian acceleration in dark matter haloes: Consequences for MOND, Physics of the Dark Universe 28 (2020) 100468. [arXiv:2008.04065](#), [doi:10.1016/j.dark.2020.100468](#).
- [81] F. Lelli, S. S. McGaugh, J. M. Schombert, SPARC: Mass Models for 175 Disk Galaxies with Spitzer Photometry and Accurate Rotation Curves, Astron. J. 152 (2016) 157. [arXiv:1606.09251](#), [doi:10.3847/0004-6256/152/6/157](#).
- [82] P. Li, F. Lelli, S. S. McGaugh, N. Starkman, J. M. Schombert, A constant characteristic volume density of dark matter haloes from SPARC rotation curve fits, Mon. Not. Roy. Astron. Soc. 482 (4) (2019) 5106–5124. [arXiv:1811.00553](#), [doi:10.1093/mnras/sty2968](#).

- [83] J. Bekenstein, M. Milgrom, Does the missing mass problem signal the breakdown of Newtonian gravity?, *ApJ*286 (1984) 7–14. [doi:10.1086/162570](https://doi.org/10.1086/162570).
- [84] M. Milgrom, Can the Hidden Mass Be Negative?, *ApJ*306 (1986) 9. [doi:10.1086/164314](https://doi.org/10.1086/164314).

Table 1: In the table, the first column gives the name of the galaxy, the second one the best fitting values of the DM surface density (obtained in [80]), and the relative errors, the third column the luminosity at $3.6 \mu\text{m}$, and the relative errors given in the SPARC’s webpage, and the fourth column the effective surface brightness given in SPARC’s webpage.

Name	$\log(\rho_{\text{DM}})(M_{\odot}/\text{pc}^3)$	$L[3.6 \mu\text{m}] (10^9 L_{\odot})$	$\Sigma_{\text{eff}}(L_{\odot}/\text{pc}^2)$
UGC02487	2.33 ± 0.23	489.955 ± 4.061	818.14
UGC02885	2.24 ± 0.11	403.525 ± 4.088	421.53
NGC6195	2.18 ± 0.1	391.076 ± 6.123	686.8
UGC11455	3.01 ± 0.11	374.322 ± 3.792	571.26
NGC5371	2.13 ± 0.09	340.393 ± 1.881	560.83
NGC2955	2.57 ± 0.11	319.422 ± 4.413	974.61
NGC0801	1.82 ± 0.06	312.57 ± 3.455	818.14
ESO563-G021	3.28 ± 0.13	311.177 ± 2.579	429.37
UGC09133	1.92 ± 0.06	282.926 ± 2.345	1284.78
UGC02953	3.64 ± 0.06	259.518 ± 0.717	1544.65
NGC7331	2.4 ± 0.06	250.631 ± 0.693	2470.76
NGC3992	2.82 ± 0.18	226.932 ± 0.836	360.44
NGC6674	1.69 ± 0.07	214.654 ± 1.977	560.83
NGC5985	3.37 ± 0.15	208.728 ± 1.538	288.95
NGC2841	2.25 ± 0.04	188.121 ± 0.52	983.63
IC4202	3.55 ± 0.06	179.749 ± 3.311	391.59
NGC5005	2.67 ± 0.21	178.72 ± 0.494	1789.91
NGC5907	2.93 ± 0.04	175.425 ± 0.646	449.6
UGC05253	2.77 ± 0.09	171.582 ± 0.79	1488.78
NGC5055	2.22 ± 0.06	152.922 ± 0.282	1383.02
NGC2998	1.94 ± 0.09	150.902 ± 2.085	479.55
UGC11914	2.95 ± 0.08	150.028 ± 0.553	2425.66
NGC3953	2.79 ± 0.45	141.301 ± 0.521	587.26
UGC12506	2.9 ± 0.07	139.571 ± 3.214	144.82
NGC0891	2.82 ± 0.06	138.34 ± 0.255	1617.45
UGC06614	2.22 ± 0.17	124.35 ± 2.52	1461.61
UGC02916	2.68 ± 0.08	124.153 ± 1.83	2425.66
UGC03205	3.06 ± 0.09	113.642 ± 1.361	587.26
NGC5033	2.65 ± 0.09	110.509 ± 0.407	2036.24
NGC4088	2.21 ± 0.15	107.286 ± 0.494	457.96
NGC4157	2.12 ± 0.1	105.62 ± 0.486	848.85
UGC03546	2.57 ± 0.11	101.336 ± 0.747	2403.42
UGC06787	1.9 ± 0.06	98.256 ± 0.543	1891.6
NGC4051	2.44 ± 0.37	95.268 ± 0.439	319.76
NGC4217	2.98 ± 0.16	85.299 ± 0.393	483.98

Table 1: Continued

Name	$\log(\rho_0 r_0)(M_\odot/pc^3)$	$L[3.6\ \mu m](10^9 L_\odot)$	$\Sigma_{eff}(L_\odot/pc^2)$
NGC3521	2.35±0.1	84.836±0.156	2232.7
NGC2903	2.82±0.2	81.863±0.151	632.16
NGC2683	2.67±0.19	80.415±0.222	1139.8
NGC4013	2.03±0.05	79.094±0.364	746.16
NGC7814	2.71±0.06	74.529±0.343	2709.13
UGC06786	2.43±0.09	73.407±0.676	992.73
NGC3877	2.88±0.11	72.535±0.401	598.18
NGC0289	1.84±0.12	72.065±0.465	1587.93
NGC1090	2.82±0.22	72.045±0.796	283.68
NGC3726	1.96±0.12	70.234±0.388	198.08
UGC09037	2.33±0.1	68.614±1.769	334.83
NGC6946	2.31±0.16	66.173±0.122	571.26
NGC4100	2.79±0.11	59.394±0.328	388
NGC3893	2.68±0.16	58.525±0.377	1573.37
UGC06973	2.98±0.11	53.87±0.347	3317.65
ESO079-G014	2.56±0.15	51.733±0.524	157.34
UGC08699	2.17±0.09	50.302±0.695	2191.95
NGC4138	2.82±0.29	44.111±0.284	1909.11
NGC3198	2.15±0.06	38.279±0.212	178.99
NGC3949	2.86±0.23	38.067±0.28	1058.84
NGC6015	1.73±0.1	32.129±0.237	331.76
NGC3917	2.44±0.1	21.966±0.202	112.94
NGC4085	2.55±0.15	21.724±0.2	856.7
NGC4389	3.03±0.22	21.328±0.216	207.41
NGC4559	2.05±0.15	19.377±0.107	211.27
NGC3769	2.25±0.12	18.679±0.189	626.37
NGC4010	2.27±0.11	17.193±0.19	14.75
NGC3972	2.48±0.12	14.353±0.172	164.75
UGC03580	2.33±0.07	13.266±0.195	614.94
NGC6503	2.26±0.03	12.845±0.059	774.16
UGC11557	2.36±0.53	12.101±0.212	106.86
UGC00128	2.18±0.1	12.02±0.565	20.36
F579-V1	2.46±0.4	11.848±0.742	56.6
NGC4183	2.38±0.18	10.838±0.15	86.46
F571-8	2.79±0.14	10.164±0.412	825.71
NGC2403	2.34±0.04	10.041±0.028	341.06
UGC06930	2.29±0.25	8.932±0.14	73.93
F568-3	2.31±0.29	8.346±0.592	23.81
UGC01230	2.5±0.54	7.62±0.379	28.63
NGC0247	2.06±0.18	7.332±0.027	33.79
NGC7793	2.01±0.16	7.05±0.026	233.79
UGC06917	2.33±0.1	6.832±0.12	53.07
NGC1003	1.7±0.09	6.82±0.075	140.87

Table 1: Continued

Name	$\log(\rho_0 r_0) (M_\odot/pc^3)$	$L[3.6 \mu m] (10^9 L_\odot)$	$\Sigma_{eff} (L_\odot/pc^2)$
F574-1	2.31±0.12	6.537±0.596	29.98
F568-1	2.54±0.21	6.252±0.564	20.36
UGC06983	2.39±0.1	5.298±0.102	53.56
UGC05986	2.43±0.15	4.695±0.048	76.71
NGC0055	1.94±0.04	4.628±0.013	54.55
ESO116-G012	2.33±0.16	4.292±0.071	90.54
UGC07323	2.01±0.25	4.109±0.042	61.49
UGC05005	1.84±0.31	4.1±0.283	25.63
F561-1	1.9±0.59	4.077±0.327	22.12
NGC0024	2.8±0.35	3.889±0.036	151.65
F568-V1	2.53±0.28	3.825±0.384	31.39
UGC06628	2.16±0.6	3.739±0.076	34.74
UGC02455	3.63±0.31	3.649±0.034	254
UGC07089	1.85±0.2	3.585±0.089	37.4
UGC05999	2.24±0.54	3.384±0.231	22.95
NGC2976	2.46±0.26	3.371±0.019	308.2
UGC05750	1.8±0.21	3.336±0.264	6.87
NGC0100	2.13±0.2	3.232±0.063	64.99
UGC00634	2.08±0.28	2.989±0.146	26.11
F563-V2	2.62±0.4	2.986±0.267	23.6
NGC5585	2±0.09	2.943±0.033	90.54
NGC0300	2.11±0.23	2.922±0.008	147.51
UGC06923	2.17±0.18	2.89±0.077	166.28
F574-2	0.74±0.5	2.877±0.384	10.89
UGC07125	1.77±0.17	2.712±0.08	28.11
UGC07524	2.04±0.07	2.436±0.025	29.71
UGC06399	2.21±0.09	2.296±0.072	30.82
UGC07151	2.28±0.09	2.284±0.025	76.71
F567-2	1.87±0.66	2.134±0.305	11.5
UGC04325	2.67±0.17	2.026±0.035	41
UGC00191	2.21±0.39	2.004±0.063	50.21
F563-1	2.38±0.25	1.903±0.17	14.22
F571-V1	1.97±0.42	1.849±0.267	15.3
UGC07261	2.44±0.47	1.753±0.048	39.16
UGC10310	2.21±0.31	1.741±0.053	28.37
UGC02259	2.51±0.17	1.725±0.038	47.08
F583-4	2.01±0.25	1.715±0.185	24.94
UGC12732	1.73±0.2	1.667±0.048	26.84
UGC06818	2.15±0.22	1.588±0.057	56.08
UGC04499	2.1±0.21	1.552±0.043	33.79
F563-V1	1±0.41	1.54±0.165	9.75
UGC06667	2.26±0.07	1.397±0.066	18.06
UGC02023	2.73±0.6	1.308±0.033	27.59

Table 1: Continued

Name	$\log(\rho_0 r_0) (M_\odot/pc^3)$	$L[3.6 \mu m] (10^9 L_\odot)$	$\Sigma_{eff} (L_\odot/pc^2)$
UGC04278	2.08±0.15	1.307±0.026	34.11
UGC12632	2.04±0.18	1.301±0.03	13.09
UGC08286	2.46±0.03	1.255±0.018	39.52
UGC07399	2.6±0.16	1.156±0.024	113.98
NGC4214	1.9±0.22	1.141±0.008	363.77
UGC05414	1.98±0.24	1.123±0.028	32.87
UGC08490	2.31±0.14	1.017±0.012	124.98
IC2574	1.69±0.12	1.016±0.012	15.88
UGC06446	2.29±0.16	0.988±0.032	37.05
F583-1	2.13±0.15	0.986±0.093	11.19
UGC11820	1.3±0.18	0.97±0.047	20.18
UGC07690	2.45±0.35	0.858±0.018	184.01
UGC04305	2.31±0.44	0.736±0.007	76.71
NGC2915	2.46±0.07	0.641±0.008	347.4
UGC05716	1.62±0.12	0.588±0.042	27.59
UGC05829	1.77±0.4	0.564±0.019	10.59
F565-V2	2.06±0.18	0.559±0.098	6.93
DDO161	1.65±0.14	0.548±0.015	20.74
DDO170	1.99±0.2	0.543±0.03	9.39
NGC1705	2.71±0.11	0.533±0.01	347.4
UGC05721	2.63±0.16	0.531±0.011	233.79
UGC08837	2.5±0.24	0.501±0.015	15.73
UGC07603	2.32±0.19	0.376±0.008	81.81
UGC00891	1.89±0.18	0.374±0.017	19.09
UGC01281	1.99±0.04	0.353±0.009	13.83
UGC09992	2.03±0.52	0.336±0.017	20.18
D512-2	1.79±0.3	0.325±0.022	9.22
UGC00731	2.06±0.11	0.323±0.019	25.63
UGC08550	2.14±0.17	0.289±0.009	45.38
UGC07608	2.18±0.47	0.264±0.012	16.48
NGC4068	2.57±0.32	0.236±0.005	30.26
NGC2366	1.9±0.06	0.236±0.005	31.98
UGC05918	1.95±0.21	0.233±0.011	5.36
D631-7	1.89±0.06	0.196±0.009	20.93
NGC3109	2±0.04	0.194±0.002	11.4
UGCA281	2.03±0.2	0.194±0.007	12.5
DDO168	2.12±0.08	0.191±0.005	18.23
DDO064	2.01±0.28	0.157±0.007	17.41
PGC51017	1.64±0.39	0.155±0.014	15.03
UGCA442	1.96±0.08	0.14±0.005	7.6
UGC07866	1.77±0.37	0.124±0.004	21.92
UGC07232	3.21±0.3	0.113±0.002	83.34
UGC07559	1.65±0.37	0.109±0.004	17.9

Table 1: Continued

Name	$\log(\rho_0 r_0) (M_\odot / pc^3)$	$L[3.6 \mu m] (10^9 L_\odot)$	$\Sigma_{eff} (L_\odot / pc^2)$
NGC6789	2.87 ± 0.32	0.1 ± 0.003	59.27
KK98-251	1.52 ± 0.32	0.085 ± 0.007	7.89
UGC05764	2.36 ± 0.15	0.085 ± 0.006	9.31
CamB	2.55 ± 0.28	0.075 ± 0.003	7.89
ESO444-G084	2.27 ± 0.22	0.071 ± 0.003	19.81
DDO154	1.86 ± 0.04	0.053 ± 0.002	19.99
UGC07577	2.18 ± 0.41	0.045 ± 0.002	11.94
D564-8	1.46 ± 0.25	0.033 ± 0.004	10.11
NGC3741	1.82 ± 0.04	0.028 ± 0.001	42.94
UGC04483	1.84 ± 0.2	0.013 ± 0.001	29.71
UGCA444	1.83 ± 0.05	0.012 ± 0	11.94